Nano Energy (2015) 13, 283–290

Available online at www.sciencedirect.com

ScienceDirect

journal homepage: www.elsevier.com/locate/nanoenergy

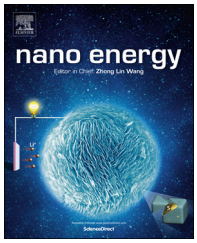

RAPID COMMUNICATION

Self-formed conductive nanofilaments in (Bi, Mn)O_x for ultralow-power memory devices

Chen-Fang Kang[a,b], Wei-Cheng Kuo[c], Wenzhong Bao[b,d], Chih-Hsiang Ho[e], Chun-Wei Huang[f], Wen-Wei Wu[f], Ying-Hao Chu[f], Jenh-Yih Juang[c], Snow H. Tseng[a], Liangbing Hu[d], Jr-Hau He[b,*]

[a]*Institute of Photonics and Optoelectronics & Department of Electrical Engineering, National Taiwan University, Taipei 10617, Taiwan, ROC*
[b]*Computer, Electrical and Mathematical Sciences and Engineering (CEMSE) Division, King Abdullah University of Science and Technology (KAUST), Thuwal 23955-6900, Kingdom of Saudi Arabia*
[c]*Department of Electrophysics, National Chiao Tung University, Hsinchu 300, Taiwan, ROC*
[d]*Department of Materials Science and Engineering, University of Maryland, College Park, MD 20742-4111, USA*
[e]*Department of Electrical Engineering, Purdue University, West Lafayette, IN 47907, USA*
[f]*Department of Materials Science and Engineering, National Chiao Tung University, Hsinchu 300, Taiwan, ROC*

Received 10 February 2015; received in revised form 24 February 2015; accepted 24 February 2015
Available online 5 March 2015

KEYWORDS
Nanofilament;
Operating energy;
Ultralow power;
Memory;
Complex metal oxide

Abstract
Resistive random access memory (RRAM) is one of the most promising candidates as a next generation nonvolatile memory (NVM), owing to its superior scalability, low power consumption and high speed. From the materials science point of view, to explore optimal RRAM materials is still essential for practical application. In this work, a new material (Bi, Mn)O_x (BMO) is investigated and several key performance characteristics of Pt/BMO/Pt structured device, including switching performance, retention and endurance, are examined in details. Furthermore, it has been confirmed by high-resolution transmission electron microscopy that the underlying switching mechanism is attributed to formation and disruption of metallic conducting nanofilaments (CNFs). More importantly, the power dissipation for each CNF is as low as 3.8/20 fJ for set/reset process, and a realization of cross-bar structure memory cell is

*Corresponding author.
E-mail address: jrhau.he@kaust.edu.sa (J.-H. He).

http://dx.doi.org/10.1016/j.nanoen.2015.02.033

demonstrated to prove the downscaling ability of proposed RRAM. These distinctive properties have important implications for understanding switching mechanisms and implementing ultralow power-dissipation RRAM based on BMO.

Introduction

The conventional charge-based memory technologies, such as dynamic random-access memory, static random-access memory and flash memory, are approaching their scaling limits due to the exponentially increased leakage current (charge loss) and the shrunk storage capability of electrons as the memory cell is scaled down [1-3]. Therefore, embedded 3D structure has been explored to provide a new knob on tackling the scaling limit [4-6]. Meanwhile, the non-charged based resistance random access memory (RRAM) with the capability of high cell density in both 2D and 3D-stacked CMOS/RRAM hybrid structure [7,8], have gained increasing attention in both science and technology communities for the past ten years [9-12].

On the other hand, different oxide materials, such as binary metal oxides, have been extensively investigated for RRAM optimization [13,14]. Although it is widely accepted that, regardless of oxide materials, the resistive switching behavior of RRAM is due to the formation and rupture of conducting nanofilaments (CNFs) in oxide, it is found that the physical origins of CNF formation in different oxide materials may not be the same. Several mechanisms have been observed and put forward to explain the causes of the CNF formation in different materials [15-22]. For example, a popularly suggested mechanism is the crystalline phase change of metal oxides, such as that a conductive ordered Ti_4O_7 phase can be transformed from single crystal TiO_2 in the Pt/TiO_2/Pt structure *via* joule heating [19]. Another explanation attributes to the oxygen diffusion induced ionic and electron conductivity change of the entire insulating layer, such as in an Au/CeO_2/Nb-STO structure [20,21]. Moreover, the mobile metal ions from one electrode can travel through solid-state electrolyte to form CNFs under the influence of electric field, such as in Pt-Ir/Cu-GeTe/Cu structure [22]. However, the details of the physical mechanisms of resistive switching are not fully understood yet and still the subject of ongoing research. Therefore a continuing exploration of new RRAM materials and corresponding resistance-switching mechanisms is still of great fundamental importance and will benefit the future development of this area. On the other hand, a superior low power performance can benefit from the downscale capability of RRAM and thus the energy consumption for switching operation of a single CNF could be an ultimate judgment of different RRAM devices [23-27]. However, no detailed studies have been conducted so far to investigate the information of CNF density in RRAM devices due to the difficulty in the observation of CNFs.

Complex metal oxides (CMO), are one of the most important materials for the application in sensors and memories [28-34], based on their unique ferroelectric, ferromagnetic, piezoelectric

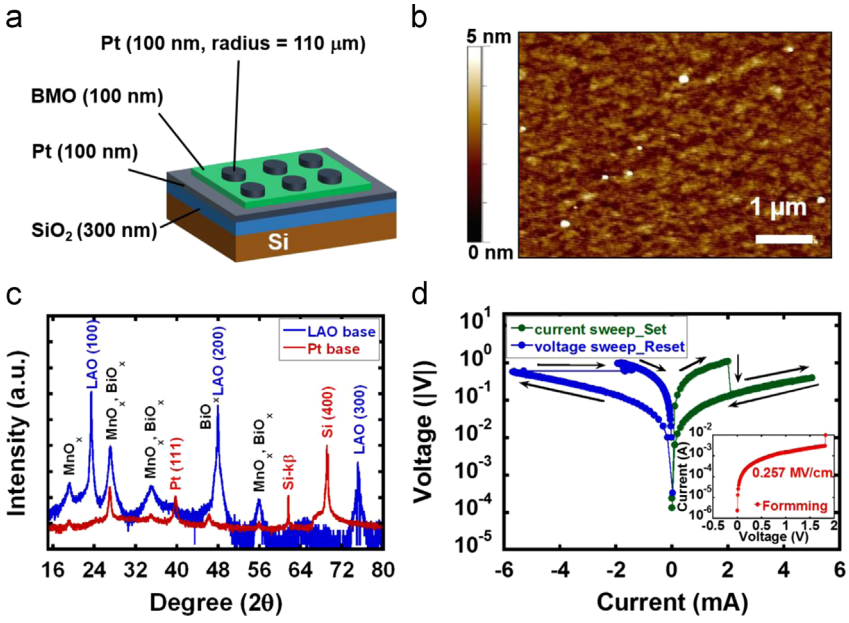

Fig. 1 (a) Schematic of the Pt/BMO/Pt structured device. (b) AFM topographical image of as-deposited BMO films. (c) XRD patterns of BMO films deposited on $LaAlO_3$ (blue) and Pt/Ti/SiO_2/Si (red) substrates at 500 °C by pulsed laser deposition. (d) Typical *I*-*V* characteristics of the Pt/BMO/Pt device in current sweep (green dots) and voltage sweep (blue dots) process. The inset shows the *I*-*V* curve of the forming process.

and thermoelectric properties. CMO such as $SrTiO_3$, $SrZrO_3$, $PrCaMnO_3$, $LaSrMnO_3$ [35–37], have been investigated for memory and logic circuitry applications, due to their stable polarization states. However, the study of CMO based RRAM is still at the early stage, and further research and discussion on various materials and mechanisms are required. In the present study, a CMO material, (Bi, Mn)O_x (BMO), commonly used as a multiferroic material [38], is applied in a Pt/BMO/Pt structured device with demonstration of resistive-switching behavior. The CNF formation in BMO thin film is revealed by high-resolution transmission electron microscopy (HRTEM), showing the CNF composed of pure Bi and Mn atoms due to electrically driven redox mechanism. The RRAM performance is also examined in detail, including forming, set and reset process, size and spacing of CNFs, and switching stability. Furthermore, the ultralow power dissipation in the BMO based devices is discussed. It is revealed that the energy for switching each CNF can be as low as 3.8/20 fJ for set/reset process, even lower than that of single wall carbon nanotube [24]. Finally, to further verify feasibility and downscaling ability of BMO-based RRAM, a cross-bar BMO RRAM array is realized.

Experimental section

To fabricate a metal-insulator-metal structured RRAM device on a SiO_2/Si substrate (Figure 1a), a 5-nm-thick Ti adhesion layer and a 100-nm-thick Pt layer were first deposited by electron-beam evaporation as a bottom electrode (BE), followed by deposition of a 80-nm-thick BMO thin film (Bi_2O_3 and MnO_2 as precursor materials) by pulsed laser deposition with a KrF laser (COMPex-pro, λ=248 nm) at 70 mTorr of oxygen background pressure and temperature at 500 °C. An atomic force microscope (AFM) was then used to characterize the surface morphology of the BMO film (Figure 1b), showing a surface roughness in nanometer scale. The X-ray diffraction (XRD) patterns of BMO thin films deposited on $LaAlO_3$ and Pt/Ti/SiO_2/Si substrates exhibit the identical peaks (Figure 1c), indicating that the main components of the BMO film are the polycrystalline MnO_x and BiO_x, which was also verified by the energy dispersive x-ray spectroscopy (EDX). Finally circular top electrodes (TEs) of 110 μm in radius (100-nm Pt) are patterned on top of the BMO film using radio frequency magnetron sputtering, assisted by a metal shadow mask. The electrical measurement of Pt/BMO/Pt devices was carried out with a Keithley 4200 semiconductor parameter analyzer at room temperature. In this work, the forward bias was defined as the current flowing from TE to BE, while the opposite direction is defined as the reverse bias.

Results and discussion

There are two operation modes for resistive switching of RRAM: bipolar operation mode (BOM) and unipolar operation mode (UOM) [39]. For UOM, the voltage polarities for set and disrupting processes are the same. The cell density in UOM is high due to the fact that RRAM can be stacked on diode selectors, leading to a small footprint $\sim 4F^2$, where F is the minimum feature size. However UOM requires a high current induced joule heating during the disrupting process (the reset operation), and thus compromise the stability of devices. On the other hand, CNFs are disrupted with reverse electric field in BOM, usually leading to an improved reliability and a lower power consumption [40]. One suggested mechanism is that oxygen ions in the oxide layer migrate along the direction of electric field, thus assisting the reset process instead of only joule heating [19,41]. The measured *I-V* characteristics for BOM is shown in Figure 1d. Before the switching operation can be accessed, a soft breakdown for the formation of CF in the metal

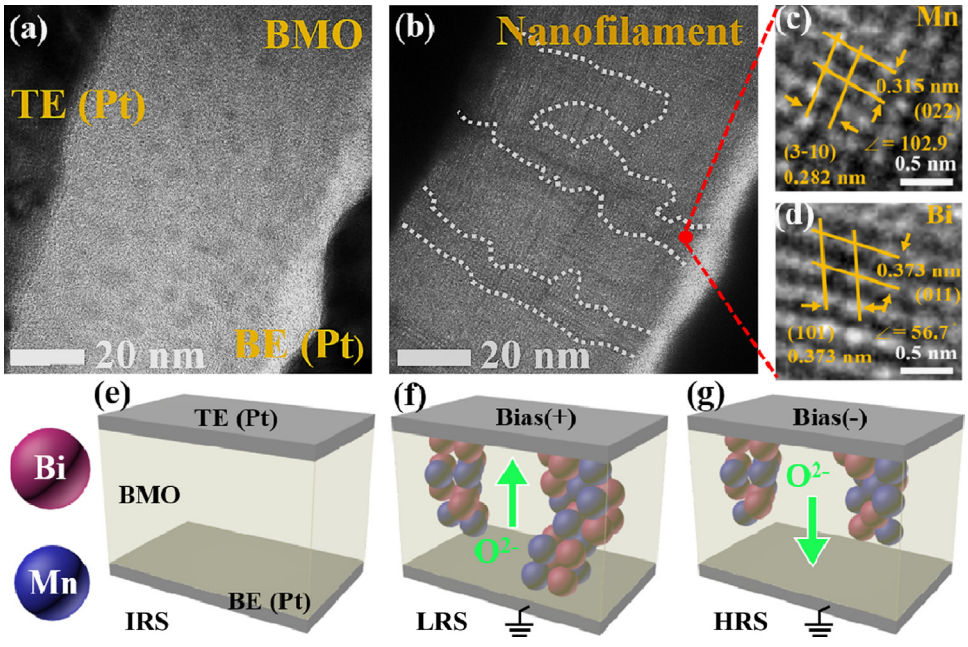

Fig. 2 (a–b) Cross-sectional HRTEM image of Pt/BMO/Pt device before and after forming proces, respectively. Notice that in (b) two intact nanofilaments connect TE and BE, and the disrupted part of the upper nanofilament is close to the BE. (c–d) HRTEM images of the Mn and Bi crystal information in the nanofilament. (e) Schematic illustration of filament structures of IRS, (f) LRS, and (g) HRS.

oxide, also known as forming process, has to be done first. As shown in the inset of Figure 1d, the current jump at 1.8 V indicates that the electrical stress induced CNF connects the two electrodes (i.e. the breakdown of oxide). After the formation of CF, the Pt/BMO/Pt device is in low resistance state (LRS), considered as a nonvolatile ON state. It is worth noting that the required electric field for establishing breakdown paths is estimated at 0.257 MV/cm for Pt/BMO/Pt device which is much lower than that for other materials reported in the previous literatures [41-43]. After the forming process, the switching operation of RRAM can now be performed. In the reset process (blue curves in Figure 1d), sweeping the voltage from 0 to −1 V results in a sudden current drop at −0.6 V (V_{reset}), indicating the switching from LRS to high resistance state (HRS, the nonvolatile OFF state of the Pt/BMO/Pt device). While in the set process, sweeping current from 0 to 5 mA (green curves in Figure 1d), a sharp voltage drop at 2 mA (I_{set}) occurred, indicating the switching of resistance state back to LRS. Here V_{reset} (around −0.6 V) is lower than V_{set} (around 1 V), while set and reset currents (I_{set} and I_{reset}) in BOM are only 2 and 6 mA, respectively. Therefore current-source sweep in the set process can avoid high compliance current, which dramatically increases the stability of resistive switching.

Figure 2a shows a cross-sectional bright-field TEM image of a fresh Pt/BMO/Pt device. No CNF can be found in the BMO layer before the forming process. Surprisingly, after the device was switched from HRS to LRS, a few CNFs with a diameter of about 10 nm, can be clearly observed between TEs and BEs, as shown in Figure 2b. To identify the material components of CNFs, the Pt/BMO/Pt device is further characterized by HRTEM for more details. Figure 2c and d clearly show d-spacing of 0.315 and 0.373 nm measured in the CF regions, corresponding to the Mn (022) and Bi (011) plane, respectively. Therefore it unambiguously verifies that the CNFs in the BMO layer are composed of Mn and Bi atoms. Hence, the deoxidization of BMO during the forming process could be responsible for the formation of CNFs in Pt/BMO/Pt device.

A schematic mechanism for CNFs formation were shown in Figure 2e-g. Figure 2e is a schematic initial resistance state (IRS) without any CNF. As the electric filed is applied, the deoxidization of BMO starts from anode side and generates CNFs. The formed CNF then shortens the gap between electrodes and hence increases current density, resulting in optimal deoxidization conditions in the region between the CF tip and cathode [44]. Therefore, the CNF extends towards cathode along the electric field with time, while the oxygen ions in the BMO migrate in the opposite direction and accumulate near the anode/BMO interface. Once the connection is set, the electrons are able to unobstructedly travel through the BMO layer assisted by Mn and Bi metal atoms crystallized in the CNF region, leading to LRS. Furthermore, a disrupted part of the CNFs is observed close to BE, as shown in Figure 2b, which can be attributed to oxidization of CNFs during the reset process. As the reverse electric field is applied, oxygen ions can migrate to the vicinity of BE/BMO interface, meanwhile the injection current produces heat along CNFs. Thus, sufficient oxygen ions and moderate operation condition together result in the oxidation of CNFs after reset process, leading to HRS. Figure 2e-g schematically illustrate the aforementioned mechanism: the electrical field induced deoxidization of BMO layer generates CNF structures which cause LRS (Figure 2f), and a reversed voltage sweep drives oxygen ions near BE back to the oxide bulk and re-oxidized Mn and Bi, thus switch the cell from LRS to HRS, as shown in Figure 2g.

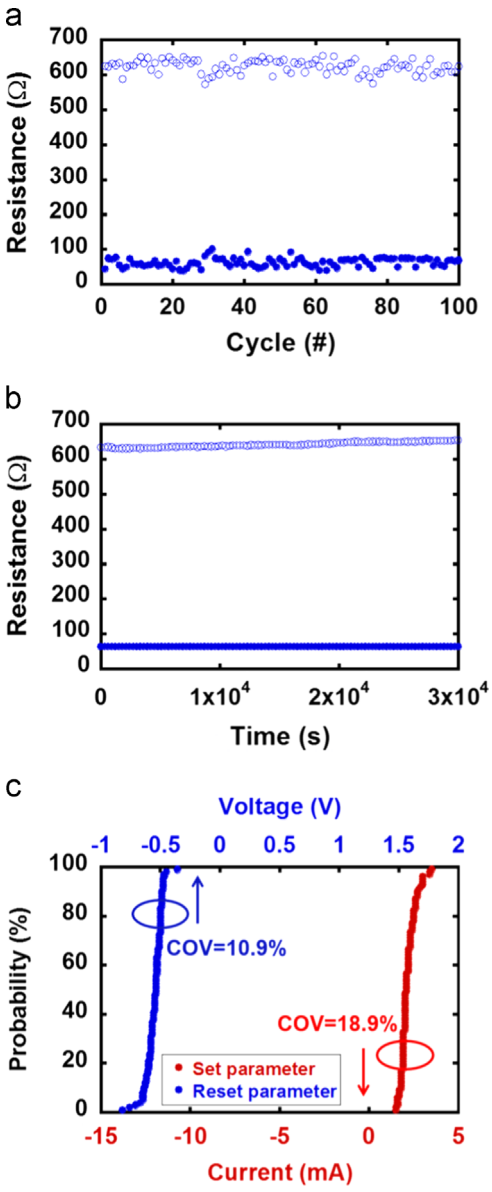

Fig. 3 (a) Resistance evolution of LRS and HRS of a Pt/BMO/Pt device within 100 switching cycles. (b) Data retention characteristic for HRS and LRS; the resistance values in HRS and LRS were read at 100 mV. (c) The distributions of I_{set} and V_{reset} of a typical Pt/BMO/P device within 100 cycles, and the COV are 18.9% and 10.9%, respectively.

To further evaluate the reliability and stability of the RRAM device, data retention and endurance characteristics were investigated. Figure 3a illustrates the evolution of LRS and HRS within 100 switching cycles. The resistance values of LRS and HRS were read out at constant voltage of 100 mV for both set or reset process. It is clear that the resistance exhibits a random distribution with a small dispersion, with

LRS ranging from 50 to 100 Ω and HRS ranging from 580 to 650 Ω, as the coefficients of variation (COV) of LRS and HRS are 20.2% and 2.98% respectively. Moreover, a superior retention capability of BMO RRAM device is demonstrated in Figure 3b, and no significant change was observed during a time scale of 3×10^4 s. The COV of switching parameters I_{set} and V_{reset} within continuous 100 switching cycles are 10.9%, and 18.9%, respectively (Figure 3c). Compared with conventional device systems such as SiO_2 and HfO_2 based RRAMs (COV of V_{set}/V_{reset} for the SiO_2 and HfO_2 are 13.5%/24.7% and 15%/28.5%, respectively) [7,45], BMO based RRAM exhibits lower operated COV and thus higher stability. Accordingly, the characteristics of low power dissipation and better reliability can be achieved in Pt/BMO/Pt device. Therefore, it validates the potential of BMO based RRAM device for NVM applications.

The density of generated CNFs at a given power is directly related to the power consumption of RRAM devices. Previous studies have shown that the distance between filaments in phase change random-access memory (PCRAM) is in the range of 0.1-5 μm [19]. Assuming that ideally one filament is enough to cause the resistive-switching, the minimum cell size for PCRAM is $100 \times 100\ nm^2$, accordingly. However, to replace the existing memory technologies, further increase of the storage density is still essential. Although various oxide materials have been studied for RRAM application, most of investigations mainly focus on a single memory cell without consideration of the storage density, or in other word, the density of CNFs. In this work, by a statistical summary of HRTEM characterizations (such as Figure 2b and Figure 4a), an average spacing of 20 ± 10 nm between adjacent CNFs can be estimated, indicating that 5 times higher density can be achieved as compared to PCRAM. As a result, the maximum cell density could reach more than 2000 cells/μm^2 in BMO RRAM devices. Another important point to emphasize here is that the average spacing of 20 nm, thus a minimum unit cell of $20 \times 20\ nm^2$ (such as illustrated in Figure 4b), is compatible with the current CMOS technologies [46].

To further estimate the power dissipation in our devices, pulsed switching data (current source, pulse width of 20 μs) collected from the cells with top electrodes with 100 μm in radius are analyzed to estimate the resistive-switching power consumption per sample area, defined as the switching energy density, e_S, to be 9.6 pJ/μm^2 and 50 pJ/μm^2 for set and reset process, respectively. Apparently lower e_S results in better power efficiency, and optimization (such as tuning of compliance current) of a particular RRAM device is usually required to achieve a minimum e_S. However, e_S is not the only coefficient to determine the power efficiency in different RRAM materials. The density of generated CNFs, α_{CF}, is also an important factor, and directly related to the downscaling ability of RRAM device for ultimate power efficiency. Obviously α_{CF} varies from one material to another, depending on the intrinsic property of each material. At a given power, a higher α_{CF} indicates lower energy to generate and switch each CF. Therefore, the energy required for creating a single CF can be written as e_S/α_{CF}, which is now a unified coefficient for characterizing the power efficiency of RRAM material. A point to emphasize here is that e_S and α_{CF} have to be measured in the same device after forming process, to eliminate the error caused by different switching operations. Accordingly, we can estimate e_S/α_{CF} in BMO based RRAM to be 3.8 and 20 fJ for set and reset process, respectively. To the best of our knowledge, few related studies have been reported, and the power-dissipation values in this work is among the lowest in previous reports which are in the order of several to hundreds of femto joules. As compared in Table 1, our result is even lower than that of a single wall carbon nanotube [23-27].

Finally to demonstrate the potential in downscaling and low cost manufacture, we fabricated and tested standalone high-density crossbar ($2\ \mu m \times 2\ \mu m$) memory array based on BMO (such as illustrated in Figure 4c). A typical *I-V* and switching characteristics of a RRAM cell with the cross-bar

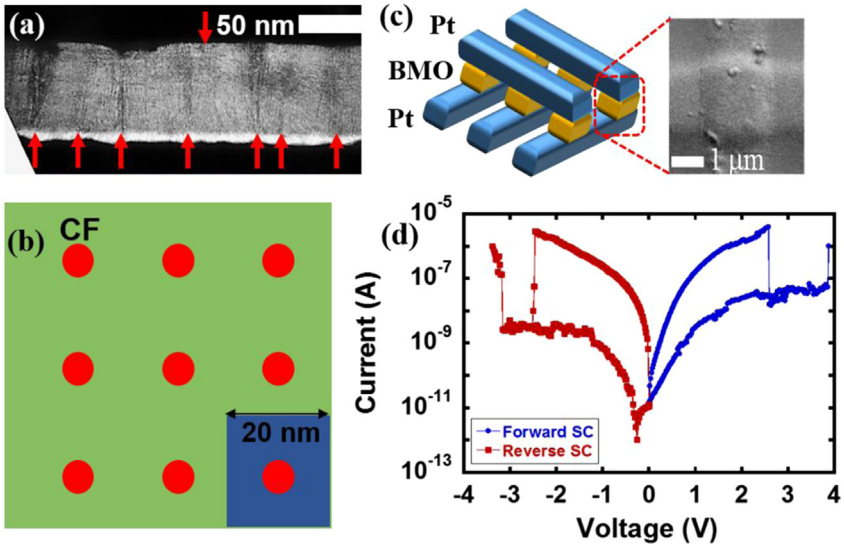

Fig. 4 (a) Cross-sectional TEM image of Pt/BMO/Pt device with 8 CNFs. (b) Schematic illustration of single filament device, and (c) a SEM image of a single unit cell with area about $2 \times 2\ \mu m^2$ within a cross-bar structure. (d) Typical *I-V* characteristics of a cross-bar structured Pt/BMO/Pt device.

Table 1 Switching energy of different memory structure.

Device Structure	Pt/BMO/Pt	Ni/GeO/HfON/TaN	Pd/CNT/Pd	Ni/GeO_x/HfON/TaN	GeO_x/NC-TiO_2/TaON	Pt/Nb_2O_5/Pt
Switching Energy (fJ)	3.8/20 (Set/reset)	6	100	8	720	40
Ref.	This study	[23]	[24]	[25]	[26]	[27]

structure is shown in Figure 4d. To consider the optimal redox conditions in BMO, as reducing the cell size, the operating energy was still fixed. Therefore, the cell needs a higher set or reset voltage for keeping an operating energy. Utilizing the above calculated e_S/α_{CF} of BMO based RRAM, we can estimate the total power consumed in such device, which is actually in the same order with the result from pulsed switching experiment. Therefore, such crossbar device suggests the feasibility of downscaling and implementation of practical memory structure and logic applications.

Conclusions

In conclusion, the 80-nm-thick BMO thin film prepared by pulsed laser deposition is first used for nonvolatile memory application. Such devices exhibit excellent resistive switching behaviors and can be operated in BOM with ultralow power consumption (i.e., 3.8 and 20 fJ for set and reset process). The CNF composed of pure metal (Mn and Bi) due to deoxidization is observed for the first time. Also, the morphology of observed CNFs with 10 nm in diameter and an average 20–30 nm spacing suggests the possibility for ultrahigh storage density application. Furthermore, excellent reliability, stability and together with a cross-bar RRAM architecture have been demonstrated to further validate the feasibility and downscaling ability of BMO-based RRAM. Thus, the low power dissipation, high cell density, reliable retention, and stable operation of Pt/BMO/Pt structured device suggest that a new member has been introduced to the RRAM family, and thus cast significant influence on future RRAM applications.

References

[1] N.S. Kim, T. Austin, D. Blaauw, T. Mudge, K. Flautner, J.S. Hu, M.J. Irwin, M. Kandemir, V. Narayanan, IEEE Comput. 36 (2003) 68–75.
[2] M.H.R. Lankhorst, B.W.S.M.M. Ketelaars, R.A.M. Wolters, Nat. Mater. 4 (2005) 347–352.
[3] S.H. Jo, W. Lu, Nano Lett. 8 (2008) 392–397.
[4] D. Lee, J. Park, J. Park, J. Woo, E. Cha, S. Lee, K. Moon, J. Song, Y. Koo, H. Hwang, Adv. Mater. 27 (2014) 59–64.
[5] H.Y. Chen, S. Yu, B. Gao, R. Liu, Z. Jiang, Y. Deng, B. Chen, F. Kang, H.P. Wong, Nanotechnology 24 (2013) 465201–465205.
[6] J.J. Ke, K.T. Tsai, Y.A. Dai, J.H. He, Appl. Phys. Lett. 100 (2012) 053503.
[7] K.L. Lin, T.H. Hou, J. Shieh, J.H. Lin, C.T. Chou, Y.J. Lee, J. Appl. Phys. 109 (2011) 084104.
[8] G.H. Kim, J.H. Lee, Y. Ahn, W. Jeon, S.J. Song, J.Y. Seok, J.H. Yoon, K.J. Yoon, T.J. Park, C.S. Hwang, Adv. Funct. Mater. 23 (2013) 1440–1449.
[9] J.Y. Seok, S.J. Song, J.H. Yoon, K.J. Yoon, T.H. Park, D.E. Kwon, H.K. Lim, G.H. Kim, D.S. Jeong, C.S. Hwang, Adv. Funct. Mater. 24 (2014) 5316–5339.
[10] D.B. Strukov, G.S. Snider, D.R. Stewart, R.S. Williams, Nature 453 (2008) 80–83.
[11] J.J. Yang, M.D. Pickett, X. Li, D.A.A. Ohlberg, D.R. Stewart, R.S. Williams, Nat. Nanotechnol. 3 (2008) 429–433.
[12] J.R. Duran Retamal, C.F. Kang, P.K. Yang, C.P. Lee, D.H. Lien, C.H. Ho, J.H. He, Appl. Phys. Lett. 105 (2014) 182101.
[13] H.S.P. Wong, H.Y. Lee, S. Yu, Y.S. Chen, Y. Wu, P.S. Chen, B. Lee, F.T. Chen, M.J. Tsai, Proc. IEEE 100 (2012) 1951–1970.
[14] Y.D. Chiang, W.Y. Chang, C.Y. Ho, C.Y. Chen, C.H. Ho, S.J. Lin, T.B. Wu, J.H. He, IEEE Trans. Electron Dev. 58 (2011) 1735–1740.
[15] G.S. Parka, X.S. Li, D.C. Kim, R.J. Jung, M.J. Lee, S. Seo, Appl. Phys. Lett. 91 (2007) 222103.
[16] F. Miao, J.P. Strachan, J.J. Yang, M.X. Zhang, I. Goldfarb, A.C. Torrezan, P. Eschbach, R.D. Kelley, G.M. Ribeiro, R.S. Williams, Adv. Mater. 23 (2011) 5633–5640.
[17] Y.C. Yang, F. Pan, Q. Liu, M. Liu, F. Zeng, Nano Lett. 9 (2009) 1636–1643.
[18] Y. Yang, P. Gao, S. Gaba, T. Chang, X. Pan, W. Lu, Nat. Commun. 3 (2012) 732.
[19] D.H. Kwon, K.M. Kim, J.H. Jang, J.M. Jeon, M.H. Lee, G.H. Kim, X.S. Li, G.S. Park, B. Lee, S. Han, M. Kim, C. S. Hwang, Nat. Nanotechnol. 5 (2010) 148–153.
[20] P. Gao, Z. Wang, W. Fu, Z. Liao, K. Liu, W. Wang, X. Bai, E. Wang, Micron 41 (2010) 301–305.
[21] P.K. Yang, W.Y. Chang, P.Y. Teng, S.F. Jeng, S.J. Lin, P.W. Chiu, J.H. He, Proc. IEEE 101 (2013) 1732–1739.
[22] S.J. Choi, G.S. Park, K.H. Kim, S. Cho, W.Y. Yang, X.S. Li, J.H. Moon, K.J. Lee, K. Kim, Adv. Mater. 23 (2011) 3272–3277.
[23] C.H. Cheng, C.Y. Tsai, A. Chin, F.S. Yeh, IEDM Tech. Dig 10 (2010) 448–451.
[24] F. Xiong, A.D. Liao, D. Estrada, E. Pop, Science 332 (2011) 568–570.
[25] C.H. Cheng, A. Chin, F.S. Yeh, IEEE Electron. Dev. Lett. 32 (2011) 366–368.
[26] M.D. Pickett, R.S. Williams, Nanotechnology 23 (2012) 215202.
[27] C.H. Cheng, A. Chin, Appl. Phys. A 111 (2013) 203–207.
[28] T.T. Kodas, Angew. Chem. Int. Ed. Engl. 28 (1989) 794–806.
[29] W. Alan Doolittle, A.G. Carver, W. Henderson, J. Vac. Sci. Technol. B 23 (2005) 1272–1276.
[30] S. Yamamoto, S. Oda, Chem. Vap. Deposition 7 (2001) 7–18.
[31] E. Strelcov, A. Belianinov, Y.H. Hsieh, S. Jesse, A.P. Baddorf, Y.H. Chu, S.V. Kalinin, ACS Nano 8 (2014) 6449–6457.
[32] H.H. Kuo, L. Chen, Y. Ji, H.J. Liu, L.Q. Chen, Y.H. Chu, Nano Lett. 14 (2014) 3314–3320.

[33] J.L. Guo, Y.D. Chiou, W.I. Liang, H.J. Liu, Y.J. Chen, W.C. Kuo, C.Y. Tsai, K.A. Tsai, H.O.H. Kuo, W.F. Hsieh, J.Y. Juang, Y.J. Hsu, H.J. Lin, C.T. Chen, X.P. Liao, B. Shi, Y.H. Chu, Adv. Mater. 25 (2013) 2040–2044.
[34] L.W. Martin, Y.H. Chu, R. Ramesh, Mater. Sci. Eng. R. 68 (2010) 89–133.
[35] Y. Watanabe, J.G. Bednorz, A. Bietsch, C.h. Gerber, D. Widmer, A. Beck, S.J. Wind, Appl. Phys. Lett. 78 (2001) 3738–3740.
[36] A. Beck, J.G. Bednorz, C. Gerber, C. Rossel, D. Widmer, Appl. Phys. Lett. 77 (2000) 139–141.
[37] C.Y. Lin, M.H. Lin, C.H. Lin, T.Y. Tseng, IEEE Trans. Electron. Dev. 54 (2007) 3146–3151.
[38] T. Kimura, S. Kawamoto, I. Yamada, M. Azuma, M. Takano, Y. Tokura, Phys. Rev. B 67 (2003) 180401.
[39] S. Yu, H.S.P. Wong, IEEE Electron. Dev. Lett. 31 (2010) 1455–1457.
[40] Z.J. Liu, J.Y. Gan, T.R. Yew, Appl. Phys. Lett. 100 (2012) 153503.
[41] W.Y. Chang, Y.C. Lai, T.B. Wu, S.F. Wang, F. Chen, M.J. Tsai, Appl. Phys. Lett. 92 (2008) 022110.
[42] A. Asamitsu, Y. Tomioka, H. Kuwahara, Y. Tokura, Nature 388 (1997) 50–52.
[43] C.Y. Lin, D.Y. Lee, S.Y. Wang, C.C. Lin, T.Y. Tseng, Surf. Coat. Technol. 203 (2008) 628–631.
[44] A.N. Grundy, B. Hallstedt, L.J. Gauckler, J. Phase Equilib. 24 (2003) 21–38.
[45] Y.T. Chen, B. Fowler, Y.F. Chang, Y. Wang, F. Xue, F. Zhou, J.C. Lee, E.C.S. Solid, State Lett. 2 (2013) 18–20.
[46] K.J. Kuhn, IEEE Trans. Electron Dev. 59 (2012) 1813–1828.

Chen-Fang Kang received the B.S. in physics at Tunghai University, Taichung, Taiwan. Then, he received his M.S. degree at National Chung Cheng University, Chiayi, Taiwan. He is currently studying toward the Ph.D. degree at the Graduate Institute of Photonics and Optoelectronics, National Taiwan University, Taipei, Taiwan. During his Master life, he has dedicated to research non-linear optics. Meanwhile, his Ph.D. is focused on exploring the resistive switching properties of novel ternary oxides.

Wei-Cheng Kuo received his B.S. & M.S. in Department of Physics from Tunghai University, Taichung, Taiwan. He is currently studying toward the Ph.D. degree at Department of Electrophysics from National Chiao Tung University, Hsinchu, Taiwan. During his Master life, he has dedicated to research Josephson Junction of YBCO superconductor. Meanwhile, his PhD is focused on investigation of mutiferroic properties in heterostructures established by different oxide thin films.

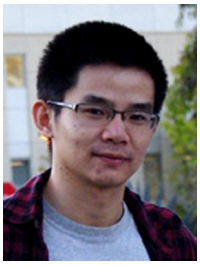

Wenzhong Bao graduated from Nanjing University with a BS in physics (2006). He received his Ph.D. from the University of California, Riverside (2011), having studied in the Department of Physics and Astronomy. He is currently a Research Associate at the University of Maryland, College Park.

Chun-Wei Huang received his M.S. degree in Materials Science and Engineering from National Taiwan Ocean University, Taiwan in 2009. He is a Ph.D. candidate in Materials Science and Engineering at National Chiao Tung University. His main research interests are preparation and applications of ZnO nanodevices, in situ TEM investigation for nanodevices.

Chih-Hsiang Ho received Ph.D. degree from the Electrical and Computer Engineering of Purdue University in 2014. He was with AU Optronics, Hsinchu, Taiwan, where he was involved in research with LCD panel design. In the summer of 2012, he worked as a graduate intern for advanced MEMS display at Qualcomm Incorporated, San Jose, CA. In the summer of 2013, he worked as a summer research intern for new reliability screening methodology at IBM T. J. Watson Research Center, Yorktown Heights, NY. His primary research interests include low-power and variation-tolerant circuit design and modeling of advanced device and circuit reliability.

Wen-Wei Wu received his Ph.D. degree in Materials Science and Engineering from National Tsing Hua University, 2003. Then he worked as Postdoctoral Fellow (2003-2008) at Materials Science and Engineering, National Tsing Hua University. He joined in Materials Science and Engineering, National Chiao Tung University from 2008. His main research interests are in situ TEM investigation of dynamical changes in nanostructured materials, synthesis metal silicide thin films and nanostructures, and metallization on Si and Si-Ge alloy.

Ying-Hao Chu received his Ph.D. in the Department of Materials Science & Engineering from National Tsing-Hua University in 2004. In 2014 he hold an adjunct position in Department of Electrophysics, National Chiao Tung University. His research is highly focused on complex functional oxides and strongly correlated electron systems. He has extensive experience in the use of advanced characterization techniques to understand and manipulate complex functional oxide heterostructures, nanostructures, and interfaces. His current goal is try to create a pathway to use topological defects for next generation electronics.

Jenh-Yih Juang Professor Juang received his B.S. & M.S. in Material Science and Engineering from National Tsing Hua University, Hsinchu, Taiwan. Ph.D. degree is Materials Science and Engineering of Massachusetts Institute of Technology, USA. In 1983 he joined National Chiao Tung University in the Department of Electrophysics as assistant associate professor, 1993 became professor and in 2002 he became an Executive Dean in College of Science His research is Experimental solid state physics Magnetic and superconducting thin films and devices Electro-optical materials.

Snow H. Tseng became an assistant professor at the Graduate Institute of Photonics and Optoelectronics of National Taiwan University in February 2006, and later promoted to associate professor in 2010. His research interests include optical interactions with biological tissues and electromagnetic wave propagation in random media.

Liangbing Hu is an assistant professor at University of Maryland College Park. His research interests include nanomaterials and nanostructures, roll-to-roll nanomanufacturing, energy storage and conversion, and printed/flexible electronics.

Jr-Hau He received his B.S. and Ph.D. degrees from the National Tsing Hua University, Hsinchu, Taiwan, in 1999 and 2005, respectively. He is currently an Associate Professor of King Abdullah University of Science and Technology (KAUST). He is involved in the design of new nanostructured architectures for nanophotonics and the next generation of nanodevices, including photovoltaics, and resistive memory. Prof. He is a recipient of the Outstanding Young Electrical Engineer Award from the Chinese Institute of Electrical Engineering (2013), the Outstanding Youth Award of the Taiwan Association for Coating and Thin Film Technology (2012), the Youth Optical Engineering Medal of the Taiwan Photonics Society (2011), and has won numerous other awards and honors with his students in professional societies and conferences internationally.